Applied Catalysis B: Environmental 221 (2018) 140–151

Contents lists available at ScienceDirect

Applied Catalysis B: Environmental

journal homepage: www.elsevier.com/locate/apcatb

Anatase photocatalyst with supported low crystalline TiO_2: The influence of amorphous phase on the activity

M.J. Torralvo[a], J. Sanz[b], I. Sobrados[b], J. Soria[c], C. Garlisi[d], G. Palmisano[d], S. Çetinkaya[e], S. Yurdakal[e], V. Augugliaro[f,*]

[a] Facultad de Ciencias Químicas, Universidad Complutense de Madrid, 28040 Madrid, Spain
[b] Instituto de Ciencia de Materiales, CSIC, C/Sor Juana Inés de la Cruz, Cantoblanco, 28049 Madrid, Spain
[c] Instituto de Catálisis y Petroleoquímica, CSIC, C/Marie Curie 2, Cantoblanco, 28049 Madrid, Spain
[d] Department of Chemical Engineering, Khalifa University of Science and Technology, Masdar Institute, Masdar City, P.O. Box 54224, Abu Dhabi, United Arab Emirates
[e] Kimya Bölümü, Fen-Edebiyat Fakültesi, Afyon Kocatepe Üniversitesi, Ahmet Necdet Sezer Kampüsü, 03100 Afyonkarahisar, Turkey
[f] "Schiavello-Grillone" Photocatalysis Group, Dipartimento di Energia, Ingegneria dell'Informazione e Modelli matematici (DEIM), University of Palermo, Viale delle Scienze, 90128 Palermo, Italy

ARTICLE INFO

Keywords:
Supported photocatalyst
Amorphous titania
Partial oxidation
^{1}H MAS-NMR
TEM

ABSTRACT

In a previous study on commercial TiO_2 nanoparticles (J. Soria et al.) we had shown that the superficial disordered layers influence their textural and reactivity features. In the present work we used well crystallized anatase particles (commercial TiO_2, BDH) as support of different amounts of titania powders, prepared by $TiCl_4$ hydrolysis and constituted by nanocrystals diluted into an amorphous matrix. The reactivity of these photocatalysts has been tested for the selective oxidation of 4-methoxybenzyl alcohol to aldehyde in aqueous suspension. The catalyst characteristics have been studied using adsorption-desorption isotherms, TEM, HRTEM, TGA, PL, DRIFT-IR, and ^{1}H MAS-NMR spectroscopy. The results show that, though amorphous titania species hinder the photocatalyst overall reactivity, the incorporation of a low amount of those species enhances significantly the reactivity towards the partial oxidation. This effect is attributed to the fact that, during the catalyst preparation, associations between chlorine ions and hydrated excess protons structures are produced. These associations act as surfactants, separating the layer of amorphous titania chains from anatase surface so that, under catalyst irradiation, the transport of photogenerated positive charge from anatase bridging oxygens to those of the amorphous layer is favoured.

1. Introduction

Since the Fujishima and Honda discovery of the photocatalytic splitting of water on a TiO_2 electrode under UV light [1], titania materials have been widely investigated and applied in energy and environment areas such as photovoltaics, photocatalysis, photo-electrochromics etc. In the case of photocatalysis the efficiency of these materials depends on the effective separation of the photo-produced holes and electrons and subsequent charge transfer reactions with adsorbed molecules, these processes being affected by many factors among which the titania particle size. In the recent decades a great research activity has been devoted to nanoscience and nanotechnology owing to the fact that interesting physical and chemical properties emerge when the size of the material is in the nanometer scale [2]. In these conditions, the specific surface area and surface-to-volume ratio drastically increase by facilitating the interaction between the material and the surrounding media. TiO_2 nanoparticles have been prepared by many methods: sol, sol-gel, micelle and inverse micelle, hydrothermal, microwave etc. [3]. In a typical sol-gel process a colloidal suspension, or a sol, is formed from the hydrolysis and polymerization reactions of the precursors, which are usually inorganic metal salts or metal organic compounds such as metal alkoxides.

In order to explore the new possibilities offered by TiO_2 nanoparticles, we prepared nanocrystalline powder by $TiCl_4$ hydrolysis at room temperature and subsequent aging treatment at 373 K for 30 min. (HP sample). The resulting semicrystalline sample was constituted by nanocrystals (mean size of 5 nm) diluted into an amorphous titania matrix, which results from the precipitation of the excess titania as a

* Corresponding author at: University of Palermo, Viale delle Scienze, 90128 Palermo, Italy.
E-mail addresses: torralvo@quim.ucm.es (M.J. Torralvo), jsanz@icmm.csic.es (J. Sanz), isobrado@icmm.csic.es (I. Sobrados), javiersoriaruiz@gmail.com (J. Soria), cgarlisi1@masdar.ac.ae (C. Garlisi), gpalmisano@masdar.ac.ae (G. Palmisano), sidikacetinkayaa@gmail.com (S. Çetinkaya), sedatyurdakal@gmail.com (S. Yurdakal), vincenzo.augugliaro@unipa.it (V. Augugliaro).

http://dx.doi.org/10.1016/j.apcatb.2017.08.089
Received 17 July 2017; Received in revised form 28 August 2017; Accepted 31 August 2017
Available online 15 September 2017
0926-3373/ © 2017 Elsevier B.V. All rights reserved.

disordered structure [4]; indeed the precursor species generated in the liquid suspension by $TiCl_4$ hydrolysis not only form crystalline oxides but also amorphous ones. The HP sample was tested for the photocatalytic oxidation of 4-methoxybenzyl alcohol (MBA) in water; the HP performance was compared with those of commercial TiO_2 samples constituted by large (mean size of ca. 60 nm) and well crystallized particles. The results [4–6] indicated that this photoprocess occurs through two parallel pathways: (i) partial oxidation to the corresponding aldehyde (p-anisaldehyde, PAA); and (ii) complete oxidation to CO_2 (mineralization) through a series of intermediates that do not desorb to the solution. The HP photoactivity was quite low owing to the fact that the amount of crystalline phase (that able to absorb photons and so to generate electron/hole pairs) was very low and that the interparticle electron transport was hindered by amorphous titania incorporation to the nanoparticles boundaries. This hindering effect favors the recombination of charge carriers in the crystalline particles where they are photogenerated [7–9]. The HP overall photoactivity, even if low, was mainly determined by the reaction towards the MBA partial oxidation product, i.e. the aldehyde. On the contrary, the well-crystallized TiO_2 samples showed a high photoactivity but mainly towards the mineralization reaction.

Partial oxidation of aromatic alcohols to corresponding aldehydes is a key step in many organic syntheses [10] whose process conditions generally involve high temperature and pressure so that the soft photocatalytic process may be a suitable alternative. With the aim of improving the partial oxidation reaction without decreasing the overall photoactivity, we planned to prepare titania catalysts by supporting HP species on anatase particles. As a preliminary study, we investigated the effect on commercial anatases (BDH and Merck TiO_2) of a strong acid treatment with HCl, this treatment being justified by the fact that HP photocatalyst is prepared in acidic conditions. The obtained results indicated that the acid treatment affects, mainly, the disordered layer at the anatase nanoparticles surface [11]. The thickness of the layer, formed by amorphous titania chains and impurities, increases and some chlorine ions, generated by HCl dissociation, are incorporated to the chains by ion exchange. Under the acid conditions of the treatment, these ions form associations with hydrated excess proton structures [12]. These structures, characterized by fast transport of positive charges [12,13], act as surfactants [14] separating the layer from the anatase particles. The excess proton delocalization in the structures, inducing their stabilization [13,15], favours its interaction with bridging hydroxyls of particles and chains.

In this work, we have prepared titania catalysts by supporting different amounts of HP on well crystallized anatase particles (commercial TiO_2, BDH) with the aim of improving the partial oxidation reaction without decreasing the overall photoactivity. These powders have been characterized by adsorption-desorption isotherms, TEM, HRTEM, TGA, PL, DRIFT-IR, and ^{1}H MAS-NMR spectroscopy and tested for the MBA photocatalytic oxidation in water.

2. Materials and methods

2.1. Catalysts preparation

The home prepared TiO_2 sample (HP) was synthesized by hydrolysis. The synthesis started with the preparation of a precursor solution at room temperature by slowly dropping 5 cm^3 of $TiCl_4$ (Fluka 98%) into a magnetically stirred beaker containing 50 cm^3 of deionised water; the pH value of the solution during the hydrolysis was about zero. After that, the beaker was closed and the mixing was prolonged for 12 h at room temperature, eventually obtaining a clear solution. After the $TiCl_4$ controlled hydrolysis, the solution was transferred to a round-bottom flask having a Graham condenser on its top. The flask was put in boiling water for 0.5 h to obtain a white suspension; at the end of this treatment, the suspension was repeatedly washed with distilled water until the achievement of neutral pH and then dried at 323 K in a rotovapor to obtain powdered photocatalyst. In three preparative runs of HP sample, commercial TiO_2 (BDH) was added to the solution before its prolonged mixing; the amount of added TiO_2 powder was chosen in order to have 85:15, 60:40 and 20:80 w:w BDH:HP mixtures. The supported TiO_2 catalysts are hereafter named BDH-HPX, being X the nominal weight percentage of HP catalyst supported on the BDH titania. In order to compare the properties of supported catalysts with those of commercial one, the BDH TiO_2 underwent the same treatment followed for the BDH-HP catalyst preparation, i.e. an HCl acid treatment and a thermal one; this sample is hereafter named BDH_{HCl}.

2.2. Photocatalytic activity determination

A Pyrex cylinder (internal radius: 1.6 cm and height: 18.8 cm) was used as photoreactor. It was irradiated by 3 external Actinic BL TL MINI 15W/10 Philips fluorescent lamps (electrical power: 15 W, radius: 0.8 cm and height: 26.5 cm) whose main emission peak is in the near-UV region at ca. 365 nm so that they behave as almost monochromatic light sources. The light sources, with their axes parallel to the photoreactor one, were put symmetrically with respect to the reactor position; the distance between the lamp axis and the photoreactor wall was 7.5 cm. When only one lamp was turned on, the radiation incident on the reactor wall was 6.50 W m^{-2}; it was measured by a radiometer Delta Ohm DO9721 with an UVA probe (315 ÷ 400 nm). The photoreactor and the lamps were put inside a box made of dark wood, so it can be assumed that light reflection from the box walls is negligible. The photoreactor was provided with ports in its upper section for the inlet and outlet of oxygen and for sampling. A magnetic stirrer guaranteed a satisfactory suspension of the photocatalyst and the homogeneity of the reacting mixture. For all the runs, the initial MBA concentration was 0.5 mM while the amount of catalyst was 0.4 g/L. Before switching on the lamp, pure oxygen was bubbled into the suspension for 30 min at room temperature to reach the thermodynamic equilibrium; the bubbling was maintained in the course of all runs. Adsorption of the alcohol under dark conditions was always quite low, i.e. ca. 3%. During the runs, samples of suspension were withdrawn at fixed time intervals; they were immediately filtered through a 0.45 μm hydrophilic membrane (HA, Millipore) before being analyzed.

The identification and quantitative determination of the species present in the reacting suspension was performed by means of a Beckman Coulter HPLC (System Gold 126 Solvent Module and 168 Diode Array Detector), equipped with a Luna 5 μ Phenyl-Hexyl column (250 mm long × 2 mm i.d.), using Sigma-Aldrich standards. Retention times and UV spectra of the compounds were compared with those of standards. The eluent consisted of 17.5% acetonitrile, 17.5% methanol and 65% 40 mM KH_2PO_4 aqueous solution. Retention times for MBA and PAA are 8.7 and 17.1 min, respectively. Total organic carbon (TOC) content was measured for evaluating the percentage of mineralization; these analyses were carried out by using a 5000 A Shimadzu TOC analyzer. All used chemicals were purchased from Sigma-Aldrich with a purity > 99.0%.

2.3. Catalyst characterization

XRD patterns were recorded at 1° min^{-1} with a Bruker D8 Advance diffractometer by using the Cu Kα radiation. For structural refinements, the PowderCell 2.4 program was used [16]. Prior to the structure refinements, a pattern matching without structural model was performed to obtain suitable profile parameters. Then, the structural model was refined with the Rietveld method keeping constant profile parameters. The crystallinity of all the samples was evaluated following the procedure reported by Jensen et al. [17]. XRD diffractograms were recorded for mixtures of TiO_2 and CaF_2 (50% by weight) and the areas of the 100% peaks of anatase (101), rutile (110) and CaF_2 (220) were determined. By comparing the ratios between the areas of (101) and (220) peaks and those of (110) and (220) peaks with respect those obtained

by using the pure phases (1.25 for anatase and 0.90 for rutile), the amount of crystalline and amorphous phases present in the samples was estimated.

Transmission electron microscopy (TEM) with a JEOL JEM 2000FX microscope (operating at 200 kV) and a JEOL 3000 High-Resolution TEM (operating at 300 kV) was used to characterize the morphology and microstructure of prepared samples. In each case, the sample was suspended in butanol and a drop of the suspension was deposited on a copper grid coated with a holey carbon support film. The time spent in analyzing different parts of samples was minimized in order to avoid modification of the samples; then, TEM analyses of different samples did not produce degradation of the particles surface.

The adsorption-desorption measurements were made in an ASAP 2020 Micromeritics equipment. Prior to the adsorption experiments, the sample was out-gassed at 383 K for 3 h. For specific surface area calculations, the value of 0.162 nm^2 has been used for the area occupied by a nitrogen molecule in a monolayer on flat surface [18]. The pore size distribution was obtained by the BJH method [19] using the Kelvin equation with the assumption of cylindrical pores [20].

The characteristic molecular vibrations of the surface groups of the prepared powders were investigated by DRIFT IR using a Bruker VERTEX 80/80 v, equipped with liquid nitrogen cooled MCT detector. Before recording the spectra, the samples were outgassed for about 12 h in a vacuum line (Quantachrome NOVA 2000e analyzer) at room temperature and 10^{-4} bar. The spectra were obtained in absorbance mode. For each spectrum, 256 consecutive scans at 4 cm^{-1} resolution were acquired in the 4000–400 cm^{-1} wavenumber range.

Photoluminescence (PL) emission spectra of the samples were measured using a Perkin Elmer LS 55 Fluorescence Spectrometer equipped with a front surface sample holder, where the powders were positioned. PL measurements were then recorded on dry powders with the following parameters: excitation wavelength: 300 nm; scanning speed of 200 nm min^{-1}; excitation slit width: 5 nm; emission slit: 10 nm.

Thermogravimetric analyses were performed in nitrogen flow by using a Netzsch STA 449 F3 thermal analysis equipment. Samples of ca. 30 mg were used and the following temperature program was applied: temperature was increased from 30 °C to 120 °C at a rate of 5 °C min^{-1} and the sample was kept at 120 °C for 15 min. Afterwards, temperature was increased from 120 °C to 750 °C at a rate of 10 °C min^{-1}. The temperature was then decreased from 750 °C back to 30 °C at a rate of 50 °C min^{-1}.

^{1}H magic angle spinning (MAS) NMR spectra were recorded after $\pi/2$ radiofrequency pulse irradiations at 400.13 MHz in an AVANCE 400 (Bruker) spectrometer (B_0 = 9.4 T). In MAS-NMR experiments, samples were spun at 10 kHz around an axis inclined 54°44′ with respect to the magnetic field. The number of scans was 100 and the time between successive experiments 5 s. Spectra were recorded for untreated, evacuated at room temperature and evacuated at 100 °C samples. A conventional vacuum line (residual pressure: 10^{-4} Torr) was used to evacuate samples. To preserve the evacuation conditions, the rotors were filled under nitrogen atmosphere inside a globe box. Spectra deconvolution was carried out with the Winfit (Bruker) software package. Chemical shift values were referred to the tetra-methyl-silane signal, and NMR lines intensities to that of the rotor cap used.

3. Results and discussion

3.1. Structural features

The XRD patterns of BDH and BDH_{HCl} samples exhibit all peaks expected for anatase reflections (JCPDS n. 78-2486); both samples showed the same patterns indicating that the acid and thermal treatment of BDH sample did not cause appreciable changes. HP and BDH-HP samples show reflection peaks of anatase and rutile (JCPDS n. 21-1276) phases, Figs. 1 and 1SM-5SM of Supporting material. The anatase peaks are formed by narrow lines; their intensity increased with the BDH content and the rutile peaks increased with HP content. The relative percentages of crystalline phases, measured with the CaF_2 method [17], are in the 18–98% range, Table 1 and Figs. 6SM–10SM. The CaF_2 method [17], even if less accurate than a recently proposed one [21], is very simple and satisfies our goal to state a correct sequence of crystallinity in analyzed samples.

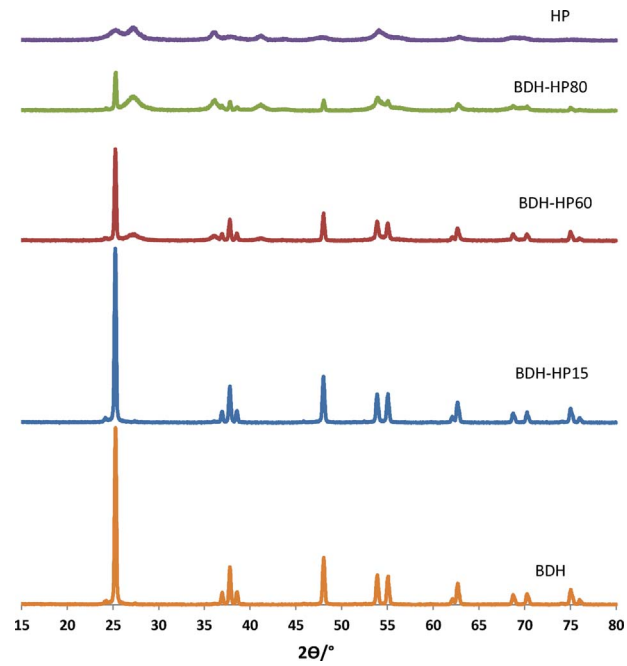

Fig. 1. XRD diffractograms of samples.

Table 1
Some features of catalysts. k_{Ov}, k_{PO} and k_{Min} are the zero order kinetic constants of MBA degradation, partial oxidation and mineralization reactions, respectively. A: anatase, R: rutile.

Catalysts	Crystals Phases	Crystallinity percentage [%]	k_{Ov} [mM*m/h]	k_{PO} [mM*m/h]	k_{Min} [mM*m/h]
BDH	A	98	1.71E-05	2.21E-06	1.49E-05
BDH_{HCl}	A	98	2.56E-05	3.06E-06	2.25E-05
BDH-HP15	A + R	86	2.04E-05	1.18E-05	8.59E-06
BDH-HP40	A + R	69	4.51E-06	3.73E-06	7.81E-07
BDH-HP80	A + R	35	1.55E-06	8.46E-07	7.03E-07
HP	A + R	19	7.98E-07	2.68E-07	5.30E-07

The anatase and rutile percentages of samples are reported in Fig. 2. The dotted lines drawn in this Figure indicate the nominal percentages of anatase and rutile in BDH-HP samples. It is interesting to note that for BDH-HP15 sample the anatase content is higher than the nominal one while rutile content is negligible. On the contrary, the other BDH-HP samples show lower anatase contents than the nominal ones corresponding to BDH and HP anatase and higher rutile contents than those corresponding to HP contributions. These features indicate that the formation process of HP nanoparticles during the BDH-HP sample preparation is affected by the presence of anatase BDH particles.

The HP synthesis carried out in the absence of BDH TiO_2 produced nanoparticles constituted by about the same percentages of anatase and rutile crystals but mainly by amorphous titania covering the crystal surface [22]. In this case, the crystal growth is hindered when amorphous titania layers cover the particle surfaces. The HP synthesis carried out in the presence of anatase BDH crystals seems to follow two different routes depending on the amount of BDH TiO_2; for both routes, however, the big BDH particles are able to incorporate HP nanoparticles

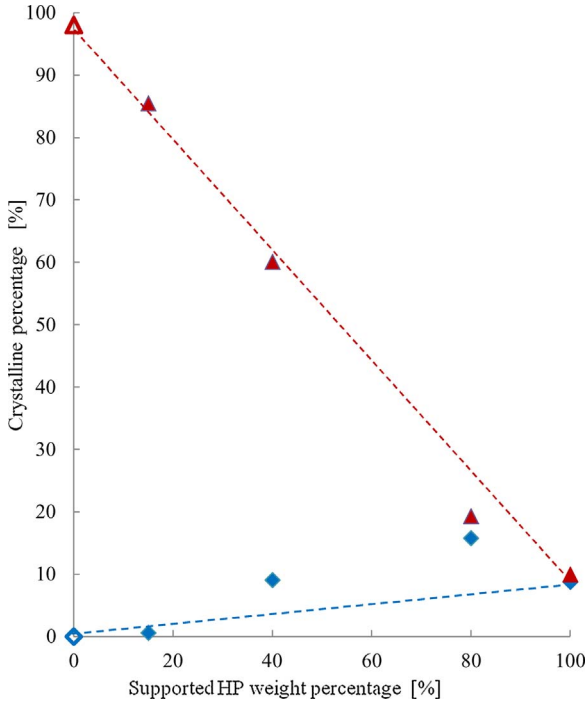

Fig. 2. Crystal percentage of anatase (▲, △) and rutile (◆, ◇). Empty symbols refer to BDH_{HCl} sample. Dotted red and blue lines indicate the anatase and rutile nominal contributions of BDH_{HCl} and HP samples, respectively, to the BDH-HP samples. (For interpretation of the references to colour in this figure legend, the reader is referred to the web version of this article.)

produced in the solution bulk. In the presence of a relatively high amount of BDH particles, the majority of HP nanoparticles produced during the course of synthesis are in the anatase phase suggesting that the BDH surface acts as anatase crystallization seed or it may easily incorporate anatase nanocrystals growing in the solution bulk. In this case the presence of a high amount of BDH anatase crystals favours the HP crystallization in the anatase phase at expense of rutile one. As in the synthesis without BDH TiO_2, amorphous TiO_2 layers cover the surfaces of resulting HP nanoparticles. When the amount of BDH crystals is low in relation with the HP one, the HP nanoparticles of BDH-HP samples show rutile and anatase percentages higher and lower, respectively, than those of HP sample alone, Fig. 2. In this case, the BDH crystals should quickly incorporate the few HP anatase crystals present in the solution bulk allowing the HP rutile crystals to grow. The rutile crystal growth is hindered by the formation of amorphous titania layers on their surface.

The TEM photographs of BDH-HP samples, reported in Fig. 3, support the XRD results. The TEM images of BDH-HP15 associations show that some anatase has grown on the BDH surface; however, only small HP particles were detected on the surface of big BDH anatase particles (top-figures). Due to the high amount of BDH particles, HP nanoparticles are not able to cover the whole crystal surface and some small HP nanoparticles appear on the BDH particles surface, mainly at their boundaries. These particles, presenting a crystal size of about 5 nm, are distributed in a more or less uniform way. In some cases the attachment of the small nanoparticles to the BDH anatase crystals takes place by a face to face approach of small nanoparticles to BDH ones, with the same orientation of their crystallographic planes. This orientating effect may act provided that the surfaces of BDH and HP crystals show very thin or no layers of amorphous titania. The attachment could take place by water-mediated H-bonding of terminal and bridging hydroxyls, displaying the most basic and acid character in surfaces of HP and BDH anatase phases [23,24]. The attachment of the other small HP particles, with different orientation of the surface planes, can take place by H-bonding of hydroxyls (terminal and bridging ones) of HP amorphous

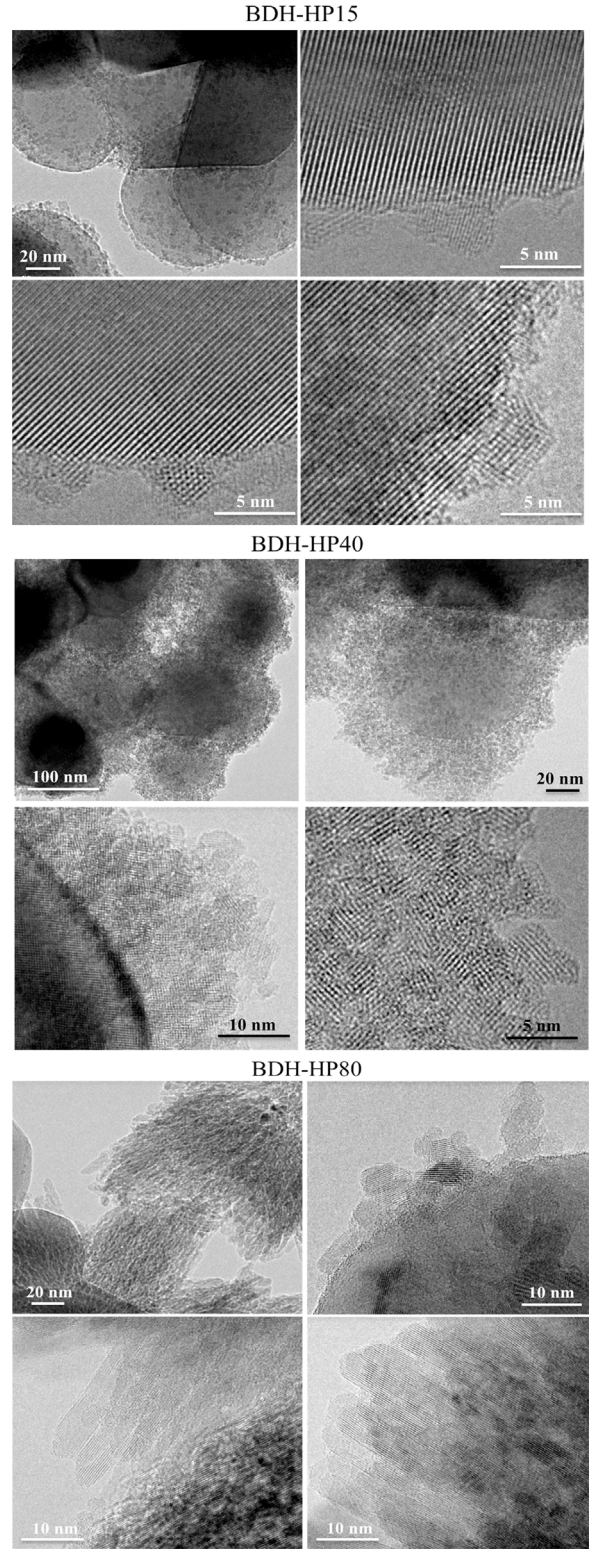

Fig. 3. TEM photographs of BDH-HP samples.

species and those of BDH particles.

The decrease of the BDH content in the preparation dispersion increases the number of small HP nanoparticles present on the BDH particles surface but not their size. In the BDH-HP40 TEM images, disordered agglomerations of small nanoparticles may be observed (middle-figures). This behaviour indicates that the majority of those nanoparticles are formed in the bulk of the preparation suspension and

that amorphous titania covering their surface is limiting the growth of crystalline cores.

By further decreasing of the BDH crystal content, self-ordered associations are developed perpendicular to the BDH particle surface. In fact, the small HP nanoparticles produced in the dispersion firstly determine the coverage of the BDH anatase particles by a layer of HP nanoparticles bonded to the BDH particle surface and, then, the bonding of new particles to those of the first layer. This second step, which starts at the places with the highest concentration of small particles, as observed in the BDH-HP80 images, takes places with a significant modification of the small particles and of the characteristics of their aggregates. Instead of appearing as particles covered by a thick layer of amorphous titania, now that amorphous layer is very thin so that the anatase BDH crystals may determine a certain orientation of semicrystalline nanoparticles. These nanoparticles do not accumulate on the BDH crystals in a random way but they form protruding wire-like structures on the crystal surface as it may be clearly noted in BDH-HP80 sample (down-figures). The near disappearance of the amorphous titania layer of HP particles suggests that during the sample preparation the strong solution acidity, together with the presence of Cl^- ions, has led to the layer elimination by the breaking of Ti-O-Ti bonds of amorphous titania chains. The breaking of these bonds should favour the mobility of the chains; in the acid solution, these chains should condense forming separate species, which could induce the observed decrease on the sample specific surface area (see later). The removal of most of the amorphous titania layer covering the crystalline core of the small HP nanoparticles favours their aggregation giving to their aggregates the appearance of a single crystal.

3.2. Textural properties

The curves of the nitrogen adsorption-desorption isotherm are of type IV, with type H1 hysteresis loop for BDH, BDH-HP15 and BDH-HP80 samples and type H3, extended down to P/P_0 value of 0.4, for BDH-HP40 and HP ones (Fig. 4). Type H1 loop is obtained with agglomerated spherical particles and type H3 isotherms are related to plate-like particles. The values of the samples BET surface area (S_{BET}), calculated using the nitrogen adsorption-desorption isotherm data, are presented in Table 2 together with the surface area and pore volume values for two pores ranges. The variation of the S_{BET} with increasing percentages of supported HP is consistent with the increasing incorporation of HP nanoparticles (2–8 nm) to the BDH crystals surface. The lower S_{BET} value of BDH-HP80 sample is consistent with the larger size of the HP nanoparticles (see Fig. 3) which probably are the result of the growth of the small ones perpendicular to the BDH particle surface.

Fig. 5 reports cumulative surface area values as a function of pore size for the HP and BDH-HP samples. For HP sample, the micropores are

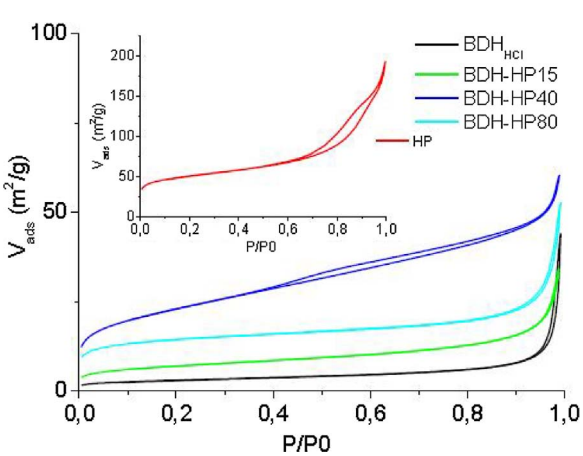

Fig. 4. Adsorption-desorption isotherms of catalysts.

responsible for about the half of its S_{BET}, pores with size in the 3–30 nm range being responsible for 65–80 m^2/g of S_{BET}. Micropores are probably located between primary particles (3–5 nm) while the pores with size in the 3–30 nm range are located among agglomerates (20–40 nm) of primary particles.

For BDH-HP15 sample, 2–4 m^2/g correspond to pores with size higher than 10–20 nm; these pores are located among the BDH titania particles with sizes is in the 50–250 nm range. Pores with sizes less than 10 nm determine the remaining S_{BET} (20–22 m^2/g); pores with 1.7–20 nm size, however, determine the majority of S_{BET}. The micropores, located between primary particles (2–5 nm), display a maximum at 3.5 nm.

For the BDH-HP40 sample only 5 m^2/g correspond to pores with size higher than 10 nm, the remaining S_{BET} is determined by pores with lesser size. As for the BDH-HP15 sample, micropores located between the primary particles display a maximum at 3.5 nm.

For BDH-HP15 and BDH-HP40 samples, most pores have a width in the range of 1.7–10 nm with maximum at 3.5 nm, representing a S_{BET} value between 20 and 76 m^2/g. Other pores present a width in the range of 10–20 nm, representing a S_{BET} of about 3 and 4 m^2/g.

These results indicate that the increase of the sample S_{BET} (BDH < BDH-HP15 < BDH-HP40, Table 1) is mainly due to the increasing incorporation of small HP nanoparticles to the surface of BDH particles. The layers of amorphous titania chains originate the smallest mesopores when small particles are attached to BDH ones and/or to other small nanoparticles. The markedly lower S_{BET} values than that of the HP sample (about 90 of the total 180 m^2/g), prepared by the same procedure but without BDH anatase particles in the preparation dispersion, and the smaller size of the small nanoparticles suggest that, though most of the initially synthesized titania chains formed very small HP particles, some of them were trapped by the BDH particles, generating micropores and small mesopores.

3.3. Thermogravimetric study

Fig. 6 reports the thermogravimetric (TG) profiles of the studied samples and Table 3 presents the values of all weight losses. The TG analysis of the BDH and BDH_{HCl} samples has been previously reported [11]. It was found that the BDH profile (not presented in Fig. 6) showed two weight losses, a small fast one at up to 395 K followed by a very small slow weight loss in the 395–550 K range, and a very small weight gain at up to 1050 K.

The profiles of BDH_{HCl}, BDH-HP and HP samples have in common a fast weight loss at up to 385 K; these losses, which represent the largest amount of water removed from each sample, can be attributed mainly to removal of water present at the outer part of the adsorbed water layer, together with weakly adsorbed water and residual Cl^- ions desorbed as HCl molecules [25].

The profile of the BDH_{HCl} sample presents three weight losses: the fast one at up to 385 K, followed by a small sharp weight loss in the 385–395 K range and a bigger slow weight loss more marked and extended than that presented by the BDH profile, up to 1043 K [11]. Because of the temperature range, the small sharp weight loss can be attributed to the desorption of water H-bonded to anatase bridging hydroxyls [26]. Therefore, this weight loss indicates that the acid treatment originates crystal defects at the anatase surface, by breaking Ti-O-Ti bonds between anatase and its covering disordered layer, favouring the formation of bridging hydroxyls there. The acid treatment also chlorinates the amorphous titania chains forming the superficial disordered layer and it favours the proton solvation of the chain bridging hydroxyls, with the formation of hydrated excess proton structures. These structures, interacting with Cl^- ions and bridging hydroxyls of anatase and amorphous chains, act as surfactants, separating the chains from the anatase surface and from other chains. The desorption of the structure water originates the third weight loss which is stronger in the BDH_{HCl} sample profile than in the BDH one [11].

Table 2
Textural properties of the used catalysts.

Catalyst	S_{BET} [m^2/g]	$S_{(1.7–10nm)}$ [m^2/g]	$S_{(10–200nm)}$ [m^2/g]	$V_{P(1.7–10nm)}$ [cm^3/g]	$V_{P(10–200nm)}$ [cm^3/g]
BDH_{HCl}	11	6	4	0.004	0.064
BDH-HP15	25	14	4	0.011	0.037
BDH-HP40	82	60	4	0.049	0.033
BDH-HP80	52	14	5	0.010	0.056
HP	180	$87_{(1.7–20\ nm)}$	$10_{(20–200\ nm)}$	$0.160_{(1.7–20\ nm)}$	$0.100_{(20–200\ nm)}$

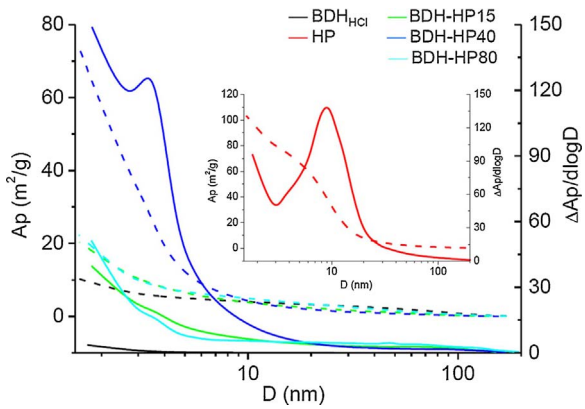

Fig. 5. Cumulative surface area (dotted line) and surface area distribution (continuous line) as a function of pore size.

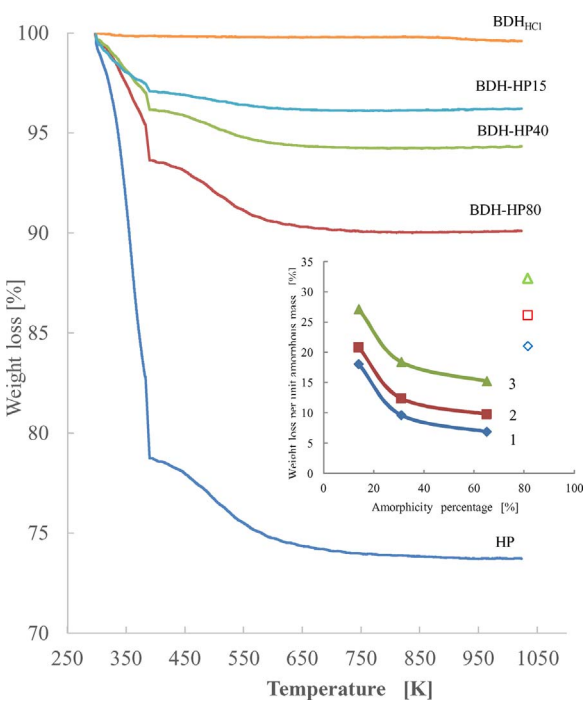

Fig. 6. Thermogravimetric profiles of BDH_{HCl}, BDH-HP and HP samples held in nitrogen flow. The inset figure shows the weight loss percentages per unit mass of amorphous content of BDH-HP samples up to 385 K (1), in the 385–395 K range (2) and in the 395–600 K range (3); the empty symbols indicate the corresponding weight losses of HP sample.

The BDH-HP40 and BDH-HP80 samples present TG profiles with four weight losses: a fast one at up to 385 K followed by the sharp weight loss in the 385–395 K range, a new weight loss in the 395–600 K range and a slow loss at up to 1016 K. All weight losses are markedly stronger than those displayed by the BDH_{HCl} profile. The similarity of these profiles indicates that the new weight loss is not related to the BDH anatase nanoparticles, but to the small and very defective rutile

Table 3
Weight losses of studied catalysts.

Catalyst	Weight loss percentage [%]			
	Up to 385 K	385–395 K	395–600 K	Up to 1016 K
BDH	0.18[a]		0.04[b]	0.04[c]
BDH_{HCl}	0.28	0.23		0.55[d]
BDH-HP15	2.52	0.38	0.8	0.1
BDH-HP40	2.98	0.85	1.8	0.1
BDH-HP80	4.49	1.88	3.5	0.1
HP	17.17	4.1	4.9	0.1

[a] Up to 395 K.
[b] 395–550 K.
[c] Weight gain in 550–1050 K.
[d] Up to 1043 K.

ones. As in the case of BDH_{HCl} sample, the acid conditions of HP sample preparation determine the breaking of Ti-O-Ti bonds between the rutile nanoparticles and their layer of amorphous titania chains. This breaking originates defects in the rutile surface, favouring the formation of bridging hydroxyls, and the separation of chains from rutile and other chains. In these samples, however, the water structures, H-bonded to bridging hydroxyls of rutile and chain clusters and acting as surfactants, contain more water and are less stable than the BDH_{HCl} sample structures. The enhancement of weight losses with increasing content of sample chains indicates that, when the chain content is too high, the dispersed chains tend to condensate by the "hydrophobic effect" [13,14], forming clusters where the protons of the remaining bridging hydroxyls are not solvated. The water structures of BDH-HP40 and BDH-HP80 samples are less rigid and less stable, but can retain more weakly adsorbed water. So, the weight loss in the 395–600 K can be attributed to the removal of H-bonded water interacting with bridging hydroxyls of rutile nanoparticles and of agglomerated chains of amorphous titania. Meanwhile, the small weight loss in the range of 600–1050 K can be due, mainly, to the removal of hydroxyls of amorphous titania chains and rutile nanoparticles.

In the case of the BDH-HP15 profile, the significant increase of the initial fast weight loss, in relation to that of the BDH_{HCl} sample, and the small weight losses observed in the temperature ranges of 385–395 and 395–600 K indicate that, at the acid conditions of the sample preparation, the amount of amorphous titania chains incorporated to the BDH nanoparticles surface is not high enough to activate the "hydrophobic effect". Most of the chains are chlorinated and incorporated to the BDH anatase surface through associations between Cl^- ions and hydrated excess protons. The TG profile of HP sample, also reported in Fig. 6, presents characteristics similar to those of BDH-HP samples but with stronger weight losses.

The inset in Fig. 6 reports the weight loss percentages per unit mass of amorphous content of BDH-HP samples up to 385 K, in the 385–395 and 395–600 K ranges as a function of the samples amorphicity; the corresponding weight losses of HP sample are also included. By considering that the weight losses of BDH_{HCl} sample are small, it may be assumed that the weight losses of BDH-HP samples are mainly determined by the amorphous part of samples. The data of Fig. 6 inset indicate that the BDH-HP losses are quite lower than the corresponding

ones of HP sample. This feature is a clear clue that the characteristics of amorphous phases of BDH-HP samples not only are different from those of HP one but also they depend on the BDH presence in the preparations. The weight loss percentages of BDH-HP samples show similar patterns; they decrease by increasing the amorphous titania content of the samples but, while the losses of BDH-HP40 and BDH-HP80 samples are similar, those of BDH-HP15 sample are quite higher. By taking into account that for BDH-HP40 and BDH-HP80 samples the "hydrophobic effect" is able to condensate the dispersed chains while for BDH-HP15 sample it does not work, the differences in the weight losses could be justified by considering that the amorphous phase of BDH-HP15 sample is different from that of BDH-HP40 and BDH-HP80 samples.

3.4. Photocatalytic activity

The activity performance of the tested samples was evaluated by determining the values of the kinetic constants of reactions occurring in studied photoprocess, i.e. that of MBA overall degradation (a parameter related to the absorbed photon flow through the quantum yield, i.e. a property of the sample bulk) and those of the MBA partial oxidation and mineralization (parameters related to the sample surface properties). Fig. 11SM reports the experimental results of a representative run.

For all the photoreactivity runs, the MBA disappearance rate, ($-r_{MBA}$), for partial oxidation and mineralization reactions in parallel, showed to obey a zero-order kinetics with respect to MBA concentration; the same kinetic law was followed by PAA and CO_2 production rates. By considering that MBA concentration is the parameter experimentally measured, the ($-r_{MBA}$) term assumes the following form:

$$(-r_{MBA}) \equiv -\frac{1}{S}\frac{dN}{dt} = -\frac{V}{S}\frac{dC}{dt} = k_{Ov} = k_{PO} + k_{Min}$$

in which S is the surface area of the catalyst, N the MBA moles, t the irradiation time, V the reaction volume, C the MBA concentration, and k_{Ov}, k_{PO} and k_{Min} are the zero-order kinetic constants of MBA overall degradation, partial oxidation and mineralization, respectively. Even if oxygen is an essential reactant for the occurrence of MBA photodegradation, its influence on the reaction rate may be omitted owing to the fact that oxygen concentration in the suspension was constant during the occurrence of MBA photooxidation. This kinetic law held for MBA conversions less than 0.5; at higher conversions, PAA molecules do compete with MBA ones for adsorption onto the catalyst surface sites for mineralization and partial oxidation. By fitting the integrated equation to the experimental data, the values of k_{Ov}, k_{PO}, and k_{Min} have been obtained. Table 1 reports the figures of k_{Ov}, k_{PO} and k_{Min}; Fig. 7 shows those kinetic constants as a function of the independent variable of our system, i.e. the supported HP percentage in the BDH-HP samples. The investigation of the structural features of BDH-HP samples showed that the HP samples incorporated to BDH-HP40 and BDH-HP80 samples are mainly constituted by rutile phase; it is assumed, hereafter, that the contribution of rutile crystals to the photoreactivity is far lesser than that of anatase ones [27]. The kinetic constant values obtained by the reactivity runs are normalized with respect to the catalyst surface area, so that they can be used for comparing the specific surface reactivity. Moreover, even if the kinetic constant depends on many operative parameters such as the photoreactor setup, the light intensity field inside the irradiated suspension, the substrate and catalyst amount, it is justified to take their value as reliable parameter for ordering the intrinsic activity of catalysts owing to the fact that the photoreactivity runs were carried out at equal irradiation and reaction conditions, the only difference being the amount of HP titania supported on BDH anatase.

The first conclusion deduced from Fig. 7 is that the BDH_{HCl} sample, i.e. the BDH sample treated in HCl solution, displays higher photoactivity than the pristine one; this improvement is determined by modifications on the surface amorphous layer as it has been deeply discussed in a previous paper [11]. The comparative analysis of the

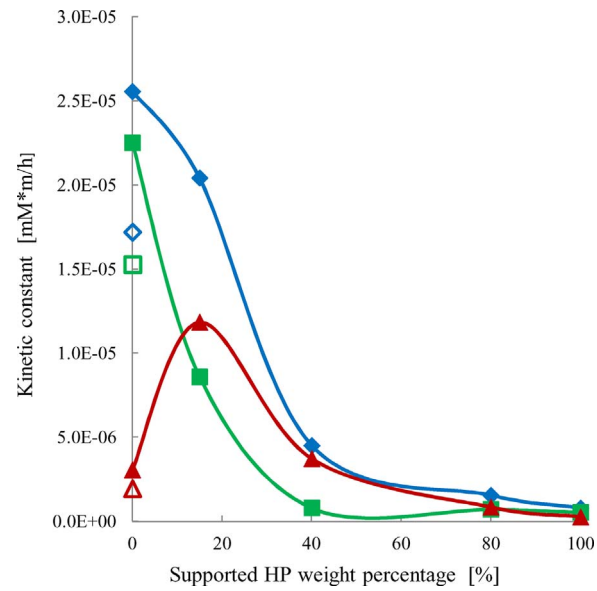

Fig. 7. The values of kinetic constants for MBA overall degradation (♦, ◇), partial oxidation (▲, △) and mineralization (■, □). Empty symbols refer to values obtained by untreated BDH sample.

photocatalytic results obtained with the BDH-HP samples shows that the BDH_{HCl} sample exhibits the highest overall photoreactivity which is mainly determined by the mineralization reaction rather than by the partial oxidation reaction. The overall reactivity decreases with increasing percentage of HP nanoparticles supported on the surface of the BDH particles. This decrease is relatively low for the BDH-HP15 anatase sample, but quite high for the BDH-HP40 and BDH-HP80 samples in which the higher content of supported HP is rutile. These results indicate that the nanoparticles of BDH-HP15 and BDH-HP40 samples and those forming the single crystal-like structures in the BDH-HP80 sample are hindering the overall photoactivity of the BDH_{HCl} particles. The decrease of the overall photoreactivity, however, is determined in a preponderant way by the strong decrease of the mineralization reaction which is affected by the low HP content in BDH-HP15 sample; at higher HP content, as for BDH-HP40 and BDH-HP80 samples, the mineralization reaction must display a value as low as that of HP sample.

The strong decrease of the mineralization reaction is compensated, in part, by the increase of the partial oxidation reaction that, initially, increases with the HP percentage incorporated to the surface of the BDH_{HCl} particles. Considering that the effect of small HP nanoparticles on the mineralization reaction is that of drastically lowering it, probably by reducing the free surface of anatase BDH crystals and/or by favouring photogenerated electron-hole recombination, the positive effect on the partial oxidation rate can be attributed to the incorporation to the BDH_{HCl} surface of anatase nanoparticles covered by low condensed amorphous titania chains.

Taking into account the strongly acid conditions of the preparation dispersion, that favor the formation of hydrated excess proton structures, and the presence of Cl^- ions, formed by $TiCl_4$ dissociation, the association of these ions to low condensed amorphous titania chains should be expected [28]. These associations act as surfactants [15], breaking Ti-O-Ti bonds between amorphous titania chains and other chains and/or anatase particles [29]. In addition, the H-bonding of these associations to BDH_{HCl} bridging hydroxyls facilitates the trapping of photogenerated holes by those hydroxyls under UV irradiation [30]. This trapping originates O^- radicals in the anatase BDH_{HCl} surface, constituting active sites for the alcohol total oxidation [31], and liberates protons to the reaction medium. The hydrated excess proton structures can also facilitate the hole transfer to the amorphous titania chains, originating active sites for the alcohol partial oxidation. So, for

BDH-HP15 sample, a catalyst containing small amounts of supported HP, the incorporation of small anatase nanoparticles to BDH_{HCl} surface has the effect of decreasing the sample photoactivity for MBA overall oxidation but the charge carriers generated in the large particles may reach the amorphous part of HP nanoparticles so improving the sample photoactivity towards the partial oxidation.

This photoactivity improving trend is, however, reverted by decreasing the BDH_{HCl} content of the samples dispersion. In this condition the HP nanoparticles formed in BDH-HP40 sample are mostly constituted by rutile crystals covered by amorphous titania chains; those nanoparticles are eventually incorporated to BDH_{HCl} particles so that, at the end of the hydrolysis process, the large particles are almost completely covered by HP nanoparticles and they contain a big amount of amorphous titania. During the sample preparation, the high amounts of the hydrated excess proton structures and of Cl^- ions favour the chain breaking and nanostructuration, forming aggregates of dense amorphous titania which act as electron-hole recombination sites. So, by increasing the HP content, the partial photo-oxidation rate firstly increases but, after reaching a maximum, it decreases so that it is not able to compensate the strong decrease of the mineralization reaction; the net effect is that the overall oxidation exhibits a sharp decrease, as observed for the BDH-HP40 sample.

Further decrease of BDH_{HCl} particles increases the time needed for HP nanoparticles incorporation. In this condition, the Cl^- ions of the preparation dispersion may induce a more marked shortening of the amorphous titania chains, to the point of being transformed into isolated Ti tetrahedra coordinated to one or more Cl^- anions. These very short chains cannot give the spherical shape to the small HP nanocrystals, but they facilitate these crystals bonding to form single crystal-like structures as observed in the BDH-HP80 TEM images. The sample photoactivity decreases to value close to those obtained using unsupported HP nanoparticles.

The photoactivity results indicate that the samples overall reactivity decreases with increasing content of amorphous phases which constitute the majority of HP nanoparticles. This consideration should induce to conclude that the presence of amorphous phase is detrimental for the photoreactivity; this is true for the overall photoreactivity but, if we consider the partial oxidation, the presence of the amorphous phase, at least until certain content, is beneficial for it. With respect to the BDH_{HCl} sample, the partial oxidation rate sharply increases after the incorporation of a small amount of dispersed HP nanoparticles, as in the BDH-HP15 sample. This increase is reverted by the decreasing sample overall photo-activity with increasing coverage of the large particles with small ones, as in the BDH-HP40 sample. For both samples, however, the contribution of partial photo-oxidation to the MBA overall degradation rate is higher than that of mineralization reaction indicating that in these samples, even if the amorphous titania content is increased, the charge carriers generated in the large particles are being transferred to the small ones whose amorphous layers are able to perform the MBA partial oxidation. This feature should indicate that, depending on the amorphous phases amount, at least two types of amorphous phases exist in those samples: the first one constitutes a thin layer of titania chains and it is active for the photoreaction occurrence while the second one constitutes thick dense layers which are not photoreactive. For this reason, by increasing the HP content and then the thick layers, the values of kinetic constants decrease and they approach figures close to those obtained using unsupported HP nanoparticles.

3.5. Interactions between anatase crystals and low crystalline titania

3.5.1. DRIFT IR

The DRIFT-IR investigation was carried out in order to study the features of water interacting with amorphous and crystalline phases. To this aim, before recording the IR spectra, the samples underwent an outgassing treatment at room temperature in a vacuum line to remove water present on the outer part of the adsorbed water layer. For this reason, while the TG results (Table 3 and Fig. 6) indicate that the water contents differ by two orders of magnitude among the samples, in the IR spectra of Fig. 8 the signal intensities of water do not show such difference.

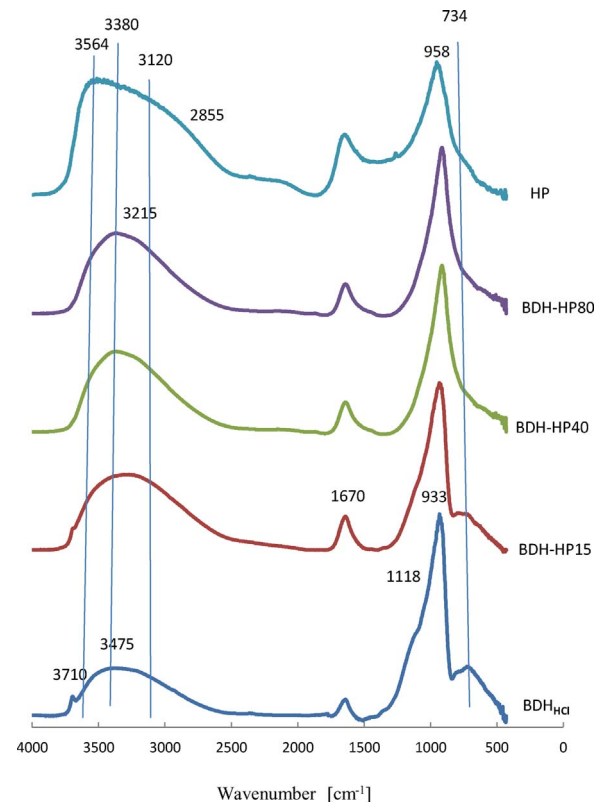

Fig. 8. DRIFT-IR spectra of all the samples recorded after outgassing for about 12 h in a vacuum line at room temperature and 10^{-4} bar.

The DRIFT-IR spectra of the BDH_{HCl}, BDH-HP and HP samples are mainly formed by two very broad absorptions, in the range of 3800-2500 and 1400–400 cm^{-1}, overlapping some narrow lines at 3710, 1670, 1118, 958, 933, and 734 cm^{-1}, Fig. 8. The absorptions at high wavenumbers are formed by several overlapped broad bands, centred at about 3475, 3380, 3215, 3120 and 2855 cm^{-1}, whose contribution to the spectrum depends on the sample composition. The band at 3475 cm^{-1} has been assigned to water molecules H-bonded to anatase bridging hydroxyls [32], while those at about 3215 and 3120 cm^{-1} have been attributed to strongly H-bonded water [33,34].

The bands in the ranges of 3250–3400 and 2700–3950 cm^{-1} can be attributed to hydrated excess protons with Zundel and Eigen structures [12,33], respectively. The solvation of protons of bridging hydroxyls, belonging most likely to amorphous titania chains, should form these structures in strongly H-bonded water of strongly acid dispersions. The higher intensity of the band at 3380 cm^{-1} than that at 2855 cm^{-1} indicates a larger contribution to the spectra of the Zundel-like form than that of the Eigen-like one. This result is consistent with those obtained by theoretical studies of water-hydrophobic wall interfaces maintained in strongly acid conditions [13]. The small band at 3710 cm^{-1} can be attributed to the free OH stretching vibrations of water at the surface of those associations [35].

In the range of the low wavenumber absorption, two regions can be considered, at 1800-1500 and 1500–400 cm^{-1}. The former is originated by overlapped narrow bands at about 1670 and 1640 cm^{-1}, which should correspond to the bending mode of water forming the hydrated excess proton Zundel-like structures [36] and of that H-bonded to those structures and to anatase bridging hydroxyls [12,36], respectively. The 1500–400 cm^{-1} range appears formed by a broad

absorption in the range of 1300–400 cm^{-1}, overlapped by several narrower bands at 1118, 958, 933, 883 and 734 cm^{-1}. Considering that the fundamental vibrations of TiO_2 nanocrystals (bands in the 550–653 and 436–495 cm^{-1} ranges, ascribed to the stretching vibrations of Ti-O and Ti-O-Ti bonds, respectively [37]) are not resolved, the absorption in the spectral range of 700–1000 cm^{-1} can be assigned to surface vibrations [35]. In the spectra of BDH_{HCl} and BDH-HP samples, the band centred at 1118 cm^{-1} has been assigned to Ti-OH vibrations [38]. The band at 734 cm^{-1}, in the range of the low wavenumber absorption, characteristic of TiO_2 surface phonons modes denoting the incomplete coordination of the surface layer ions [39], is partially shifted towards higher frequencies. This shift indicates changes in the phonon spectra of the surface TiO_2 octahedrons induced by the incorporation of water or other molecules to the coordination sphere of surface Ti cations. So, the shift of the band at 734 cm^{-1}, attributed to the stretching mode of TiO_2 bridged Ti-O bonds [40,41], is produced by the incorporation of HP species to the BDH surface and it indicates that this incorporation induces a deformation of the anatase bridging hydroxyls that favours the formation of hydrated excess protons. Meanwhile, the broad absorption in the range of 1300–400 cm^{-1} can be attributed to lattice vibrations of condensed amorphous titania chains, because of its broader linewidth [42]. In addition, the strong narrow band at 933 appears where the vibration modes of peroxide species, Ti—O—O—Ti, are usually observed [39]. This species might be formed on BDH titania by O_2 reduction during the sample synthesis [40].

The BDH-HP15 spectrum presents the high wavenumber absorption maximum at the lowest wavenumber of the reported spectra, at about 3300 cm^{-1}, and the smallest contribution of the band at 3475 cm^{-1}, indicating that this sample contains the most strongly H-bonded water [34] and that most of the BDH anatase bridging hydroxyls are interacting with hydrated excess protons structures instead of with isolated water molecules. The Cl^- ions in the dispersed amorphous titania chains should attract a substantial number of solvating water molecules. This correlation between amorphous titania chains, Cl^- ions and hydrated protons impedes the occurrence of the strong hydrophobic phase separation in concentrated acid solutions. The lower contribution of band at 734 cm^{-1} in the BDH-HP15 spectrum than in the BDH_{HCl} one and the disappearance of the band at 3475 cm^{-1} indicate that the incorporated amorphous titania chains are preferentially covering the surface of the BDH anatase particles instead of forming agglomerates of chains. However, the decrease of the broad absorption indicates that some chains do it.

The spectra of BDH-HP40 and BDH-HP80 samples show the increase of the band at 3475 cm^{-1} and the disappearance of the one at 734 cm^{-1}. These modifications suggest that, when the amount of amorphous titania chains incorporated to the BDH anatase surface is too high, the "hydrophobic effect" takes place. Non-polar chains should have a notable tendency to self-aggregate in polar solvents such as water, forming a separated phase [38,43]. The incorporation of aggregated chains to the BDH anatase surface should favour the formation of amorphous titania thick aggregates on it, leaving some empty places where water molecules can be H-bonded to anatase bridging hydroxyls. Under the strongly acid conditions, the BDH anatase interaction with the thick amorphous titania clusters can favour their transformation into rutile nanoparticles, but they do not favour the formation of Cl^- ions- hydrated excess proton associations and are very active electron-hole recombination sites during the photocatalytic reactions.

3.5.2. Photoluminescence

Fig. 9 reports PL emission spectra of samples in the wavelength range of 310–560 nm. The PL emissions result from the recombination of photo-generated electrons and holes so these spectra can be a useful tool to investigate their fate and, particularly, their separation efficiency [44,45]. In the visible range, these spectra show emission peaks at about 420, 456, 482, 520 and 541 nm, presenting similar intensity in the BDH-HP15, BDH_{HCl} and BDH spectra, while the intensity was a little higher in the BDH-HP40 spectrum and much higher in HP and BDH-HP80 samples. The strongest PL emission appears at 420 nm; it has been attributed to the transition of electrons from states in the proximity of CB to states in the vicinity of VB. This emission wavelength corresponds to energy of 2.95 eV, which does not match 3.22 eV, i.e. the band gap energy of anatase crystals: the reasons behind this difference can be seen in the nanostructured and defective character of the studied samples. The smaller peaks observed at lower energies in the 440–550 nm range appear as a result of PL excitons which result from surface oxygen vacancies and defects of the TiO_2 samples; the excitons are produced by recombination taking place at lattice defects of the crystals, which are particularly relevant in nanostructured materials. The PL peaks at 456 nm is attributed to band edge free excitons, and the other peak at 482 is attributed to bound excitons [45]. Considering that, conventionally, the higher the recombination rate is, the stronger PL peak results [46], the observed variation of the PL emission peaks in the visible range indicates that the incorporation of more than 15% of HP species to the BDH sample favours the recombination of charge carriers photogenerated by UV light. The extent of HP has an incremental effect on the integrated area of this intensity, highlighting that the amorphous rich HP boosts band-to-band recombination.

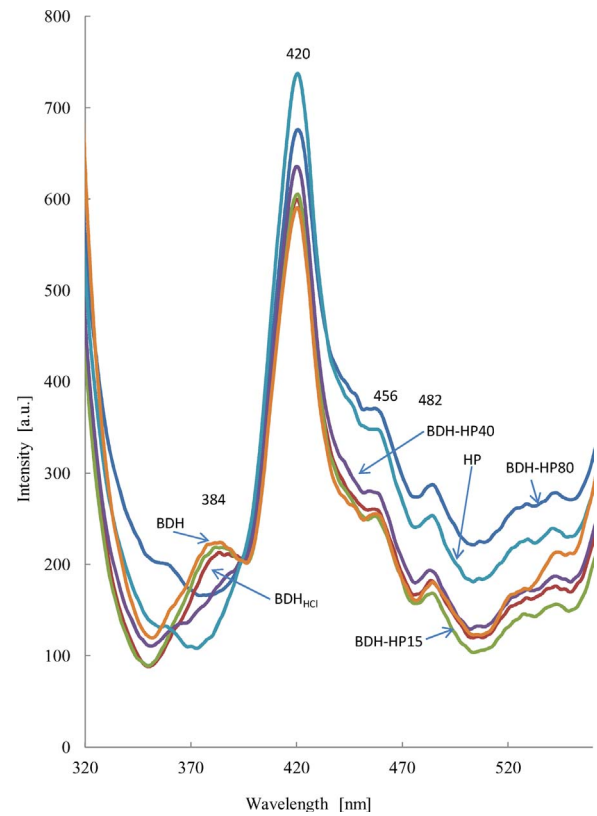

Fig. 9. Photoluminescence spectra of all the samples.

On the other hand, a high energy broad PL emission peak in the UV range, centred at about 384 nm, appears with significant intensity in the spectra of the samples with the lowest amorphous titania content, with intensity following the BDH > BDH-HP15 > BDH_{HCl} sequence. This sequence indicates that the phenomenon originating this emission peak improves the separation of photogenerated charge carriers, this improvement being more linked to the BDH acid treatment than to the incorporation of a low amount of HP species. This improvement justifies the overall photoactivity of samples. This band displays very low intensity in the BDH-HP40 spectrum and it is not observed in the BDH-HP80 and HP ones. The width of this band and the presence of shoulders suggest the presence of several overlapped peaks.

On the basis of the PL spectra features, the most noticeable effect,

related to charge carrier separation taking place in the samples with low amorphous titania content, is the increment of the photoactivity for MBA partial oxidation, following the sequence BDH < BDH_{HCl} < BDH-HP15. As the active sites for the MBA partial oxidation are holes trapped by amorphous titania bridging oxygen ions, forming O^- radicals, and the holes are photogenerated in anatase, the improvement of the partial oxidation photoactivity can be achieved by increasing the number of active sites and/or by improving the hole transfer from anatase bridging oxygens to amorphous titania chains. In a previous work, we have proposed the formation in amorphous titania chains of chlorine ions associations with hydrated excess proton structures, that act as surfactants [11]. These structures are H-bonded to bridging hydroxyls of anatase particles and amorphous titania chains forming the disordered layer on the anatase particle surface. The proton delocalization stabilizes these structures, whose main characteristic is their fast proton transport [13,15,47]. So, the band at 384 nm can be attributed to the emission of band gap transition with the energy of light approximately equal to the bandgap energy of anatase (387.5 nm). The overlapped peaks forming that PL band can correspond to the emissions originated by recombination of holes delocalized at the bridging hydroxyls of anatase particles and amorphous titania chains in the hydrated excess proton structures.

3.5.3. MAS-NMR

The ^{1}H-MAS-NMR spectroscopy, a technique able of discerning hydroxyl characteristics of sample components [48], has been previously used by our group in order to study possible interactions among different components of commercial and home prepared titania nanoparticles [11,23,24,49].

A previous study [11], carried out on BDH, BDH_{HCl} and HP samples, showed that their ^{1}H-MAS-NMR spectra are mainly formed by a strong band (denoted line W, hereafter). In the hydrated BDH spectrum, the broad line W is centred at 5.8 ppm. This chemical shift is similar to that observed for line W in the spectra of highly hydrophilic hydrated anatase samples (denoted samples HT, hereafter) with crystal size lower than 12 nm [23]. However, the width of line W, assigned to highly mobile water averaging the chemical shift of the sample hydroxyls, was much lower in HT sample spectra, about 1 ppm, than in the BDH sample, indicating a higher amount of mobile water in HT anatases. In BDH sample, the line W deconvolution showed that it is formed by two overlapped components at 5.1 and 6.5 ppm, ascribed to bridging and terminal hydroxyls in well crystallized anatase samples with low amorphous titania content [23,24]. The ^{1}H MAS-NMR spectrum of the BDH_{HCl} sample showed a narrowed line W, shifted to 6.4 ppm. This observation can be explained by partial elimination of terminal hydroxyls during acid treatment of anatase sample. The HP sample spectrum also displayed a broad line W centred at 6.5 ppm, ascribed to adsorbed water interacting with bridging OH groups of anatase, and smaller bands at 10 and 1 ppm ascribed to OH groups of titania amorphous phases. The interaction of anatase bridging hydroxyls with water favours formation of hydronium species at 7 ppm, that could still be shifted towards more positive values when interacting with basic oxygens of titania particles.

Fig. 10 shows the ^{1}H MAS-NMR spectra of the BDH-HP samples. The BDH-HP15 sample spectrum shows the main component at 6.3 ppm, suggesting, in agreement with IR results, the presence of some bridging OH groups interacting with water molecules to give hydrated excess proton structures [11,50]. The presence of additional water should favour the formation of Zundel and Eigen species and the progressive delocalization of protons in anatase samples. The BDH-HP40 sample spectrum shows a strong line W, narrower than in BDH-HP15, indicating a higher proton mobility induced by water. In this sample, the line W narrowing could be attributed to protons exchange between water and bridging hydroxyls of anatase or amorphous titania. In this sample, the TEM analysis showed that anatase nanoparticles were surrounded by amorphous layers that impeded the particles growth but

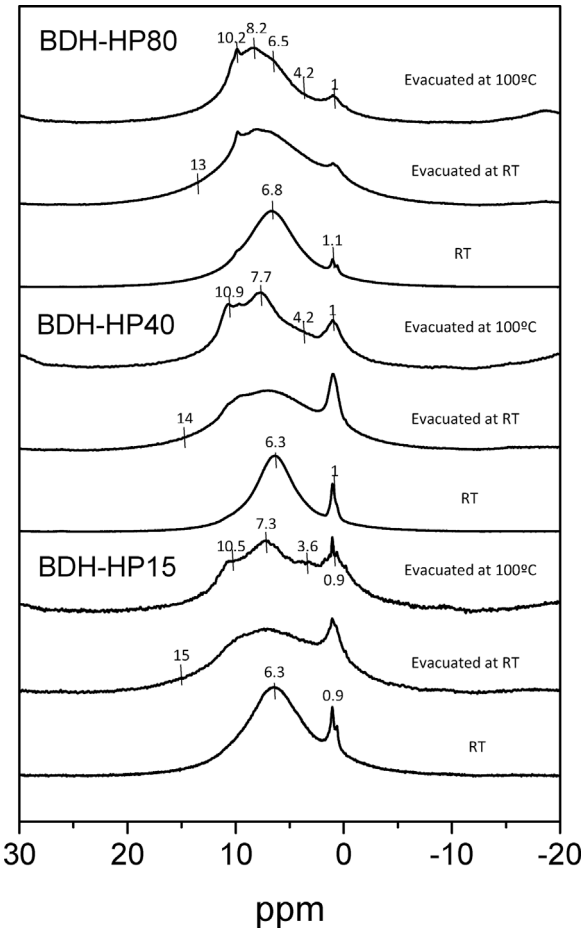

Fig. 10. ^{1}H MAS NMR spectra of BDH-HP samples.

favoured the agglomeration of titania particles.

The ^{1}H MAS-NMR spectrum of BDH-HP80 sample shows features similar to those reported previously in titania HP samples formed in acidic media [49]. In particular, small bands at 10 and 1 ppm, ascribed to amorphous segregated titania and amorphous layers that cover anatase particles. In segregated titania, the detection of an enlarged component at 15 ppm, in samples evacuated at RT, suggests that part of hydroxyls strongly interacts with neighbouring particles in self-ordered agglomerates. This band disappears in samples evacuated at 100 °C. In amorphous agglomerates, amorphous layers are deposed at the surface of anatase particles, hindering electron transfer between contiguous particles; this arrangement decreases the sample photoactivity. It is important to remark that in BDH-HP80 agglomerates most supported titania adopt the rutile form.

The $TiCl_4$ hydrolysis in presence of BDH TiO_2 particles leads to the incorporation of crystalline and amorphous particles to the surface of BDH anatase particles, inducing modifications on their surface characteristics. In particular, the incorporation of chlorinated titania species to the superficial amorphous layers of BDH particles favours the detection of a narrow new band at ~ 1 ppm. Acid treatment leads to the breaking of Ti-O-Ti bonds and the formation of new OH groups bonded to Ti cations. The presence of chlorine anions during the preparation of BDH-HP samples favours the exchange of OH^- by Cl^- ions in Ti-OH bonds, stabilizing five or fourfold coordinated Ti cations in less condensed dispersed titania chains. In these chains, the chemical shift of terminal formed OH groups is near 1 ppm. In agreement with this idea, the intensity of 1 ppm band, ascribed to chains interacting with anatase particles, should decrease further in BDH-HP80 sample which displays a higher content of amorphous aggregates than BDH-HP15 and BDH-HP40 samples. Taking into account that OH bands near 1 ppm

correspond to amorphous layers on the anatase surface, it is reasonable to admit that intensity of this band is related to the surface of anatase particles, decreasing considerably in BDH-HP80 sample.

When BDH-HP samples are outgassed at RT and 100 °C, several peaks were detected in ^{1}H MAS-NMR spectra, Fig. 10. In these samples, part of water is eliminated and detected components must be attributed to hydroxyl groups, interacting with water or oxygen atoms of contiguous titania phases. In samples evacuated at 100 °C, the resulting envelope, ascribed to anatase particles, shifted from 7.3 to 7.7 and finally to 8.2 ppm in BDH-HP15, BDH-HP40 and BDH-HP80 samples, respectively. This shift has been ascribed to anatase particles interacting with increased amounts of amorphous particles [23]. On the other hand, the weak lines at ~10, 4 and 1 ppm of amorphous phases increase at expenses of those of well-crystallized anatases. The lines at ~10 and 4 ppm have been ascribed to bridging and terminal hydroxyls of amorphous titania aggregates; however, the line at 1 ppm has been ascribed, as mentioned before, to terminal OH groups of highly defective titania sheets that interact with BDH anatase particles.

By taking into account the different intensity of 10 and 1 ppm components in samples with increasing amounts of HP, it can be deduced the presence of two types of amorphous phases, that affect in different ways the charge transfer between anatase particles. The line at 1 ppm indicates the presence of thin layers of dispersed amorphous titania chains; these layers allow the charge transfer between anatase particles and are active for photoreaction occurrence. The line at 10 ppm shows the existence of thick aggregates of dense amorphous materials that hinder electron transfer between neighbouring particles and are not photocatalytically active. According to this observation, photocatalytic activity decreases slightly in BDH-HP15 but strongly in BDH-HP80 sample.

4. Conclusions

In titania nanoparticles prepared at low temperature the coexistence and arrangement of crystalline and amorphous phases play an important role in determining the bulk and superficial characteristics. High crystallinity drastically enhances the overall photocatalytic reactivity while the amorphous phase decreases it [51,52]. While in crystalline TiO_2 the number of lattice defects decreases facilitating the electron transport, in amorphous phases the defects behave as recombination centres for the photogenerated electron/hole pairs [52].

The results of the present investigation show that the morphological and photocatalytic characteristics of samples prepared by incorporating HP species (amorphous titania chains and highly defective small crystalline TiO_2 nanoparticles) to the surface of BDH anatase nanoparticles markedly depend on the amount of those species. If the amount of incorporated HP species is small, the resulting amorphous phases are low condensed and they appear dispersed on the BDH anatase nanoparticles, forming part of their surface disordered layer. The strongly acid conditions of the BDH-HP15 preparation dispersion favour the formation of associations between Cl^- ions and hydrated excess proton structures that, acting as surfactants, separate the amorphous titania chains from the surface of anatase nanoparticles, as observed in BDH and BDH_{HCl} samples [11]. The fast transport of positive charges in the hydrated excess proton structures can facilitate the transfer of photogenerated holes from bridging oxygens of anatase particles to those of superficial amorphous titania chains. This transfer originates the active sites for the partial photocatalytic oxidation. The higher content of chains in BDH-HP15 than in BDH_{HCl} justifies its higher photoactivity towards partial oxidation. This sample has also incorporated some very defective small crystalline TiO_2 nanoparticles to the BDH particle surface. These nanoparticles, acting as electron-hole recombination sites, hinder the sample overall photoactivity.

When the amount of HP species incorporated to the surface of BDH particles reaches a certain value, the influence of the BDH anatase is so low that the "hydrophobic effect" starts to be effective. The amorphous titania chains start to condense weakening their ability of interacting with the BDH particles through the formation of associations between Cl^- ions and hydrated excess protons; this process eventually produces dense amorphous phases covering the crystal surfaces as thick layers. In addition, very small rutile nanoparticles, attached to the BDH anatase, start to form small agglomerates. These effects, observed in the BDH-HP40 sample, originate the marked decrease of partial and overall photoactivity. Further increase of HP species incorporation to BDH anatase surface, as in the BDH-HP80 sample, produces an increase of rutile nanoparticle size and of their agglomeration, originating structures protruding perpendicular to the BDH particle surface. These modifications produce a further decrease of the partial and overall oxidation photoactivity.

In conclusion, the presence of amorphous oxides, which usually are considered to have a negligible or no influence on the final properties of samples, may affect in a considerable way their structure and reactivity properties. This effect is not exclusive of photocatalytic nanoparticles; in thermal catalysis, many catalysts are prepared by applying catalytically active species to the support surface. If the supporting procedure, generally carried out at low temperature, does not imply a further thermal treatment, it is likely that amorphous phases are still present on the surface of catalysts affecting their performances.

Acknowledgements

J.Sa. thanks the Spanish Agency CICYT (project MAT2013-46452-C4-2R) and the regional Government (project MATERYENER3-CM S2013/MIT-2753) for financial support. S.Y. wishes to thank Eng. Hakan Şahin (Teknoloji Uygulama ve Araştırma Merkezi (TUAM), Afyon Kocatepe University, Turkey) for XRD analysis.

This research did not receive any specific grant from funding agencies in the public, commercial, or not-for-profit sectors.

Appendix A. Supplementary data

Supplementary data associated with this article can be found, in the online version, at http://dx.doi.org/10.1016/j.apcatb.2017.08.089.

References

[1] A. Fujishima, K. Honda, Electrochemical photolysis of water at a semiconductor electrode, Nature 238 (1972) 37–38.
[2] G. Redmond, D. Fitzmaurice, M. Graetzel, Effect of surface chelation on the energy of an intraband surface state of a nanocrystalline titania film, J. Phys. Chem. 97 (1993) 6951–6954.
[3] X.B. Chen, S.S. Mao, Titanium dioxide nanomaterials: synthesis, properties, modifications, and applications, Chem. Rev. 107 (2007) 2891–2959.
[4] G. Palmisano, S. Yurdakal, V. Augugliaro, V. Loddo, L. Palmisano, Photocatalytic selective oxidation of 4-methoxybenzyl alcohol to aldehyde in aqueous suspension of home-prepared titanium dioxide catalyst, Adv. Synth. Catal. 349 (2007) 964–970.
[5] V. Augugliaro, H. Kisch, V. Loddo, M.J. López-Muñoz, C. Márquez-Álvarez, G. Palmisano, L. Palmisano, F. Parrino, S. Yurdakal, Photocatalytic oxidation of aromatic alcohols to aldehydes in aqueous suspension of home prepared titanium dioxide 1. Selectivity enhancement by aliphatic alcohols, Appl. Catal. A 349 (2008) 182–188.
[6] V. Augugliaro, H. Kisch, V. Loddo, M.J. López-Muñoz, C. Márquez-Álvarez, G. Palmisano, L. Palmisano, F. Parrino, S. Yurdakal, Photocatalytic oxidation of aromatic alcohols to aldehydes in aqueous suspension of home prepared titanium dioxide 2. Intrinsic and surface features of catalysts, Appl. Catal. A 349 (2008) 189–197.
[7] K. Zimny, T. Roques-Carmes, C. Carteret, M.J. Stébé, J.L. Blin, Synthesis and photoactivity of ordered mesoporous titania with a semicrystalline framework, J. Phys. Chem. C 116 (2012) 6585–6594.
[8] N. Kopidakis, N.R. Neale, K. Zhu, J. van de Lagemaat, A.J. Frank, Spatial location of transport-limiting traps in TiO_2 nanoparticle films in dye-sensitized solar cells, Appl. Phys. Lett. 87 (2005) 202106.
[9] P. Docampo, S. Guldin, U. Steiner, H.J. Snaith, Charge transport limitations in self-assembled TiO_2 photoanodes for dye-sensitized solar cells, J. Phys. Chem. Lett. 4 (2013) 698–703.
[10] T. Mallat, A. Baiker, Oxidation of alcohols with molecular oxygen on solid catalysts, Chem. Rev. 104 (2004) 3037–3058.
[11] J. Soria, J. Sanz, M.J. Torralvo, I. Sobrados, C. Garlisi, G. Palmisano, S. Çetinkaya,

S. Yurdakal, V. Augugliaro, The effect of the surface disordered layer on the photoreactivity of titania nanoparticles, Appl. Catal. B: Environ. 210 (2017) 306–319.
[12] N. Agmon, Structure of concentrated HCl solutions, J. Phys. Chem. A 102 (1998) 192–199.
[13] S. Iuchi, H. Chen, S. Paesani, G.A. Voth, Hydrated excess proton at water-hydrophobic interfaces, J. Phys. Chem. B 113 (2009) 4017–4030.
[14] H. Chen, J. Xu, G.A. Voth, Unusual hydrophobic interactions in acidic aqueous solutions, J. Phys. Chem. B 113 (2009) 7291–7297.
[15] M.K. Petersen, S.S. Iyengar, T.J.F. Day, G.A. Voth, The hydrated proton at the water liquid/vapor interface, J. Phys. Chem. B 108 (2004) 14804–14806.
[16] W. Kraus, G. Nolze, POWDER CELL- A program for the representation and manipulation of crystal structures and calculation of the resulting X-ray powder patterns, J. Appl. Crystallogr. 29 (1996) 301–303.
[17] H. Jensen, K.D. Joensen, J.E. Jørgensen, J.S. Pedersen, E.G. Søgaard, Characterization of nanosized partly crystalline photocatalysts, J. Nanoparticle Res. 6 (2004) 519–526.
[18] F. Rouquerol, J. Rouquerol, K. Sing, Adsorption by Powders and Porous Solids, Academic Press, London, 1999.
[19] E.P. Barret, L.G. Joyner, P.P. Halenda, The determination of pore volume and area distributions in porous substances. I. Computations from nitrogen isotherms, J. Am. Chem. Soc. 73 (1951) 373–380.
[20] J.C. Broekhof, J.H. De Boer, Studies on pore systems in catalysts: XII. Pore distributions from the desorption branch of a nitrogen sorption isotherm in the case of cylindrical pores A. An analysis of the capillary evaporation process, J. Catal. 10 (1968) 368–376.
[21] V.A. Lebedev, D.A. Kozlov, I.V. Kolesnik, A.S. Poluboyarinov, A.E. Becerikli, W. Grünert, A.V. Garshev, The amorphous phase in titania and its influence on photocatalytic properties, Appl. Catal. B: Environ. 195 (2016) 39–47.
[22] S. Yurdakal, V. Augugliaro, J. Sanz, J. Soria, I. Sobrados, M.J. Torralvo, The influence of the anatase nanoparticles boundaries on the titania activity performance, J. Catal. 309 (2014) 97–104.
[23] J. Soria, J. Sanz, I. Sobrados, J.M. Coronado, M.D. Hernández-Alonso, F.J. Fresno, Water-hydroxyl interactions on small anatase nanoparticles prepared by the hydrothermal route, J. Phys. Chem. C 114 (2010) 16534–16536.
[24] J. Soria, J. Sanz, I. Sobrados, J.M. Coronado, M.D. Hernández-Alonso, F.J. Fresno, FTIR and NMR study of the adsorbed water on nanocrystalline anatase, J. Phys. Chem. C 111 (2007) 10590–10596.
[25] J.G. Li, M. Ikeda, Ch. Tang, Y. Moriyoshi, H. Hamanaka, T. Ishigaki, Chlorinated nanocrystalline TiO_2 powders via one-step Ar/O_2 radio frequency thermal plasma oxidizing mists of $TiCl_3$ solution: phase structure and photocatalytic performance, J. Phys. Chem. C 111 (2007) 18018–18024.
[26] M. Egashira, S. Kawasumi, S. Kagawa, T. Seiyama, Temperature programmed desorption study of water adsorbed on metal oxides. I. Anatase and rutile, Bull. Chem. Soc. Jpn. 51 (1978) 3144–3149.
[27] T. Luttrell, S. Halpegamage, J.-G. Tao, A. Kramer, E. Sutter, M. Batzill, Why is anatase a better photocatalyst than rutile?—Model studies on epitaxial TiO_2 films, Sci. Rep. 4 (2014), http://dx.doi.org/10.1038/srep04043 Art. N. 4043.
[28] H. Zhang, B. Chen, J.F. Banfield, G.A. Waychunas, Atomic structure of nanometer-sized amorphous TiO_2, Phys. Rev. B 78 (2008) 214106.
[29] I. Siretanu, J.P. Chapel, C. Drummond, Water-ions induced nanostructuration of hydrophobic polymer surfaces, ACS Nano 5 (2011) 2939–2947.
[30] J. Soria, J. Sanz, I. Sobrados, J.M. Coronado, F. Fresno, M.D. Hernandez Alonso, Magnetic resonance study of the defects influence on the surface characteristics of nanosize anatase, Cat. Today 129 (2007) 240–246.
[31] M.A. Henderson, Structural sensitivity in the dissociation of water on TiO_2 single-crystal surfaces, Langmuir 12 (1996) 5093–5098.
[32] K.S. Finnie, D.J. Cassidy, J.R. Bartlett, J.L. Woolfrey, IR spectroscopy of surface water and hydroxyl species on nanocrystalline TiO_2 films, Langmuir 17 (2001) 816–820.
[33] M. Park, I. Shin, N.J. Singh, K.S. Kim, Eigen and Zundel forms of small protonated water clusters: structures and infrared spectra, J. Phys. Chem. A 111 (2007) 10692–10702.
[34] L.F. Scatena, M.G. Brown, G.L. Richmond, Water at hydrophobic surfaces: weak hydrogen bonding and strong orientation effects, Science 292 (2001) 908–912.
[35] T. Bezrodna, G. Puchkovska, V. Shymanovska, J. Baran, H. Ratajczak, IR-analysis of H-bonded H_2O on the pure TiO_2 surface, J. Mol. Struct. 700 (2004) 175–181.
[36] J. Kim, U.W. Schmitt, J.A. Gruetzmacher, G.A. Voth, N.E. Scherer, The vibrational spectrum of the hydrated proton: comparison of experiment, simulation, and normal mode analysis, J. Chem. Phys. 116 (2002) 737–746.
[37] K. Chhor, J.F. Bocquet, C. Pommier, Syntheses of submicron TiO_2 powders in vapor liquid and supercritical phases, a comparative study, Mater. Chem. Phys. 32 (1992) 249–254.
[38] D.A. Panayotov, J.T. Yates Jr., Depletion of conduction band electrons in TiO_2 by water chemisorptions— IR spectroscopic studies of the independence of Ti-OH frequencies on electron concentration, Chem. Phys. Lett. 410 (2005) 11–17.
[39] R. Nakamura, A. Imanishi, K. Murakoshi, Y. Nakato, In situ FTIR studies of primary intermediates of photocatalytic reactions on nanocrystalline TiO_2 films in contact with aqueous solutions, J. Am. Chem. Soc. 125 (2003) 7443–7450.
[40] S. Neubert, D. Mitoraj, S.A. Shevlin, P. Pulisova, M. Heimann, Y. Du, G.K.L. Goh, M. Pacia, K. Kruczała, S. Turner, W. Macyk, Z.X. Guo, R.K. Hockingg, R. Beranek, Highly efficient rutile TiO_2 photocatalysts with single Cu(II) and Fe(III) surface catalytic sites, J. Mater. Chem. A 4 (2016) 3127–3138.
[41] J.B. Kinney, R.H. Staley, Reactions of titanium tetrachloride and trimethylaluminum at silica surfaces studied by using infrared photoacoustic spectroscopy, J. Phys. Chem. 87 (1983) 3735–3740.
[42] B.C. Trasferetti, C.U. Davanzo, Berreman effect applied to phase characterization of thin films supported on metallic substrates: the case of TiO_2, Phys. Rev. B 64 (2001) 125404.
[43] C. Tanford, The hydrophobic effect and the organization of living matter, Science 200 (1978) 1012–1018.
[44] J.G. Yu, L.F. Qi, M. Jaroniec, Hydrogen production by photocatalytic water splitting over Pt/TiO_2 nanosheets with exposed (001) facets, J. Phys. Chem. C 114 (2010) 13118–13125.
[45] Q.J. Xiang, K.L. Lv, J.G. Yu, Pivotal role of fluorine in enhanced photocatalytic activity of anatase TiO_2 nanosheets with dominant (001) facets for the photocatalytic degradation of acetone in air, Appl. Catal. B: Environ. 96 (2010) 557–564.
[46] C. Kumar (Ed.), UV-VIS and Photoluminescence Spectroscopy for Nanomaterials Characterization, Springer-Verlag, Berlin, 2013.
[47] O. Markovitch, H. Chen, S. Izvekov, F. Paesani, G.A. Voth, N. Agmon, Special pair dance and partner selection: elementary steps in proton transport in liquid water, J. Phys. Chem. B 112 (2008) 9456–9466.
[48] A.Y. Nosaka, T. Fujiwara, H. Akutsu, Y. Nosaka, Characteristics of water adsorbed on TiO_2 photocatalytic systems with increasing temperature as studied by solid-state ^1H NMR spectroscopy, J. Phys. Chem. B 108 (2004) 9121–9125.
[49] J. Sanz, J. Soria, I. Sobrados, S. Yurdakal, V. Augugliaro, Influence of amorphous TiO_{2-x} on titania nanoparticles growth and anatase-to-rutile transformation, J. Phys. Chem. C 116 (2012) 5110–5115.
[50] M.J. Cánovas, I. Sobrados, J. Sanz, J.L. Acosta, A. Linares, Proton mobility in hydrated sulfonated polystyrene. NMR and Impedance studies, J. Membr. Sci. 280 (2006) 461–469.
[51] V.F. Stone Jr., R.J. Davis, Synthesis characterization, and photocatalytic activity of Titania and Niobia mesoporous molecular sieves, Chem. Mater. 10 (1998) 1468–1474.
[52] B. Ohtani, Y. Ogawa, S. Nishimoto, Photocatalytic activity of amorphous-anatase mixture of titanium(IV) oxide particles suspended in aqueous solutions, J. Phys. Chem. B 101 (1997) 3746–3752.